Fault-tolerant Control of Six-phase Induction Motor Drives with Variable Current Injection

Ignacio González-Prieto[1], Mario. J. Duran[1], Federico J. Barrero[2]

***Abstract*— Three-phase machines are the industry standard for electrical drives, but the inherent fault tolerance of multiphase machines makes them an attractive alternative in applications requiring high reliability. For this reason different fault-tolerant control schemes for multiphase drives have been recently suggested, proving their capability to perform a ripple-free operation after an open-circuit fault occurrence. Nevertheless, the post-fault strategies proposed so far consider a single mode of operation and do not allow a high-performance braking process in drives with unidirectional power flow where regenerative braking is not possible. This work firstly explores the possibility of enhancing the braking process by using a proper injection of circulating currents that prevent the active power to reach the dc-link capacitor. This novel strategy is then combined with minimum losses and maximum torque criteria to obtain a variable current injection method that minimizes the drive derating, reduces the copper losses and improves the braking transients. Experimental results confirm the successful performance in the different zones for the case of a six-phase induction motor drive.**

***Index Terms*— Multiphase drives, induction motors, fault tolerance, open-circuit faults, braking methods.**

NOMENCLATURE

FOC	Field oriented control.
IM	Induction machine.
LM	Loss manipulation.
ML	Minimum loss.
MMF	Magneto-motive force.
MT	Maximum torque.
OCF	Open-circuit fault.
PWM	Pulse width modulation.
VSC	Voltage source converter.
VSD	Vector space decomposition.
a	Derating factor.
$e_{d,q}$	Decoupling terms.
$i_{a1,b1,c1,a2,b2,c2}$	Stator phase currents.
I_{dc}	DC-link current.
$i_{\alpha,\beta s}$	Stator currents in the α-β subspace.
$i_{x,ys}$	Stator currents in the x-y subspace.
$i_{0_+,0_-s}$	Stator currents in the 0_+0_- subspace.
$i_{\alpha,\beta r}$	Rotor currents in the α-β subspace.
i_{dsn}	Stator rated direct current.
$i_{d,qs}$	Direct and quadrature currents.
$i^*_{d,qs}$	Direct and quadrature reference currents.
I_k	rms currents in the healthy phases.
I_n	Rated rms current.
V_{dc}	DC-link voltage.
$v_{\alpha,\beta s}$	Stator voltages in the α-β subspace.
$v_{x,ys}$	Stator voltages in the x-y subspace.
$v^*_{d,qs}$	Direct and quadrature reference voltages.
$v^*_{a1,b1,c1,a2,b2,c2}$	Stator phase reference voltages.
$v_{0_+,0_-s}$	Stator voltages in the 0_+0_- subspace.
L_{ls}	Stator leakage inductance.
L_{lr}	Rotor leakage inductance.
L_m	Magnetizing inductance.
L_s	Stator inductance.
L_r	Rotor inductance.
M	Mutual inductance.
p	Number of pole pairs.
P_{DC}	DC-link power.
P_{loss}	Motor losses.
P_{shaft}	Shaft power.
R_s	Stator resistance.
R_r	Rotor resistance.
T_e	Electrical torque.
T_{load}	Load torque.
T_{shaft}	Shaft torque.
β	Friction coefficient.
ξ	Current injection factor.
ω_m	Mechanical speed.
ω_r	Rotor electrical speed.

Manuscript received July 18, 2016; revised September 16, 2016; accepted December 5, 2016.

This work was supported by the Spanish Ministry of Science and Innovation under Project ENE2014-52536-C2-1-R.

I. Gonzalez-Prieto and M.J. Duran are with the Department of Electrical Engineering at the University of Malaga, Spain, e-mail:ignaciogp87@gmail.com and mjduran@uma.es.

F. Barrero is with the Department of Electronic Engineering at the University of Seville, Spain, e-mail: fbarrero@us.es.

I. Introduction

The principle of economy, typically postulated as "*It is futile to do with more things that which can be done with fewer*", was already popular in 13th-century among the scholastic philosophers. This standard has found widespread use in the engineering context where simplicity is a key goal and products are designed to be just as good as they need to be. It is for this reason that industry is reluctant to increase the level of complexity, unless clearly justified. Focusing in the field of electric machines and drives, the law of parsimony, together with the economy of scales, makes the use of three-phase machines a default choice in industry

applications [1]. A higher number of phases are only justified if the performance is significantly improved, and for this reason that many efforts have been recently made to explore the benefits that can be obtained with the use of multiphase systems [2-5]. Otherwise the Ockham's razor would shave the extra phases away.

In this scenario, the mere extension of three-phase techniques to multiphase drives becomes insufficient and it is of paramount importance to explore the innovative uses of the additional degrees of freedom [5-11]. In other words, it is essential to highlight what can be done with a multiphase machine that is impossible to do with its three-phase counterpart. Two of these innovative modes of operation include the fault-tolerant control with no extra hardware [8-10] and the regulation of circulating currents to enhance the braking transient in topologies with diode front-end rectifiers [11].

The inherent fault tolerance provided by the phase redundancy is regarded as the main attractive feature of multiphase machines [5]. A niche of applications, including wind energy systems [12,13], electric traction [14] and more-electric aircraft [15], are already making use of this capability to improve the drive robustness. The main idea is that the system can still operate in the event of a single open-circuit fault (OCF) using the remaining $n-1$ phases ($n>3$), provided that the control strategy is adequately reconfigured after the fault detection [16]. Since the loss of a phase must be compensated increasing the current amplitude of the healthy phases, a certain derating of the drive becomes mandatory after the fault occurrence [17].

The derating can be minimized using the maximum torque (MT) mode of operation [8,10], but unfortunately it leads to higher copper losses caused by the injection of secondary currents. A minimum loss (ML) criterion has also been suggested for the post-fault operation [18,19], but it results in unequal phase current amplitudes that increase the derating of the drive if it is operated with currents below rated values. However, both MT and ML criteria assume that the motor is consuming active power.

Even though this is the normal case in motoring mode, the deceleration during braking transients can only be increased by reversing the active power to the mains. If regenerative braking is not allowed, as it is the typical case in topologies with diode front-end rectifiers, this active power elevates the dc-link voltage eventually causing the capacitors breakdown [20].

In order to speed up the braking transients without additional hardware (e.g. braking resistors), a recently presented method makes use of the secondary currents to manipulate the stator copper losses [11]. The controlled dissipation diverts the active power into Joule losses and avoids the dc-link over-voltages. A similar idea has been also used in three-phase drives with the flux-braking concept [21-22], but the use of the additional degrees of freedom allows a simple and independent loss manipulation (LM) mode of operation.

While ML and MT modes of operation have been independently used in previous works, the extension of the LM mode of operation to fault-tolerant drives is still missing. Aiming to fill this gap this work presents two main contributions:

- The extension of the LM technique to the post-fault situation.
- The definition of a global fault-tolerant strategy that integrates ML, MT and LM modes of operation.

The unified solution provides an optimum post-fault operation that maximizes the torque production, minimizes the copper losses and permits a good dynamic performance during braking transients. Even though this unified solution can be applied to any multiphase machine, this work focuses on the case of a six-phase drives supplied from two three-phase two-level voltage sources converters (VSCs). By and large multiple three-phase ($3k$) machines preserve the benefits of multiphase machines while reusing the well-established three-phase technology, lowering the barriers to entry the industrial market.

The paper structure is as follows. Section II the ML and MT fault tolerant modes of operation, section III extends the LM mode of operation to fault-tolerant drives and section IV combines the ML, MT and LM modes into a unified control strategy with variable current injection. This global strategy is experimentally tested in section V and the main conclusions are summarized in section VI.

II. Fault-tolerant Modes of Operation in Six-phase Drives

A. Six-phase drive generalities

The drive studied in this work consists of a six-phase induction machine supplied by two IGBT-based two-level three-phase VSCs connected in parallel to the same dc-link. The dc-link is in turn supplied from the grid through a diode rectifier that only allows unidirectional power flow (Fig. 1a). The motor is an asymmetrical-type machine with two three-phase windings ($a_1b_1c_1$ and $a_2b_2c_2$) whose spatial shifting is 30° and whose neutral points are isolated (Fig. 1b with $\delta = 2\pi/3$ and $\gamma = \pi/6$). The generalized Clarke matrix for this specific case is:

$$[T] = \frac{1}{\sqrt{3}} \begin{bmatrix} 1 & -\frac{1}{2} & -\frac{1}{2} & \frac{\sqrt{3}}{2} & -\frac{\sqrt{3}}{2} & 0 \\ 0 & \frac{\sqrt{3}}{2} & -\frac{\sqrt{3}}{2} & \frac{1}{2} & \frac{1}{2} & -1 \\ 1 & -\frac{1}{2} & -\frac{1}{2} & -\frac{\sqrt{3}}{2} & \frac{\sqrt{3}}{2} & 0 \\ 1 & -\frac{\sqrt{3}}{2} & \frac{\sqrt{3}}{2} & \frac{1}{2} & \frac{1}{2} & -1 \\ 1 & 1 & 1 & 0 & 0 & 0 \\ 0 & 0 & 0 & 1 & 1 & 1 \end{bmatrix} \quad (1)$$

$$\left[i_{\alpha s}\ i_{\beta s}\ i_{xs}\ i_{ys}\ i_{0+}\ i_{0-} \right]^T = [T] \cdot [\, i_{a1}\ i_{b1}\ i_{c1}\ i_{a2}\ i_{b2}\ i_{c2}\,]^T,$$

and it is used to decompose the phase variables into two subspaces, namely the α-β and x-y ones, plus the zero sequence component 0_+-0_-. The first two subspaces are orthogonal, and consequently they can be independently controlled in healthy operation. On the other hand in the

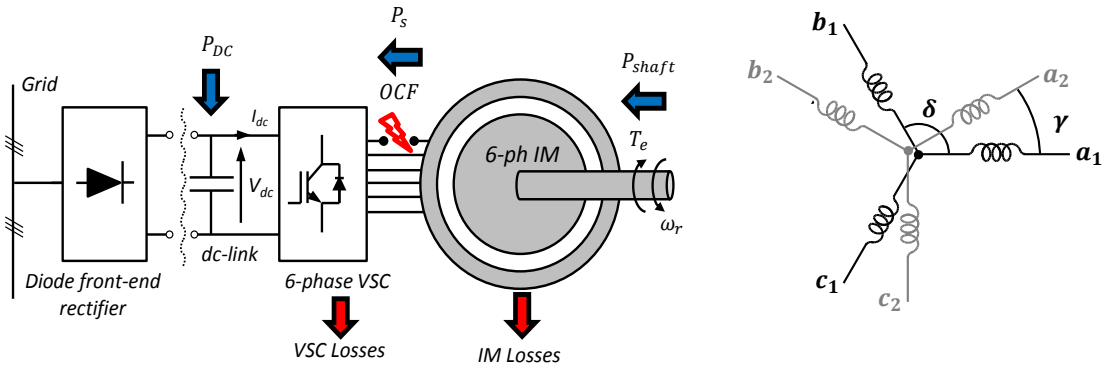

(a) (b)

Fig. 1. a) Six-phase drive topology, b) six-phase induction motor with a generic spatial shifting γ between three-phase windings.

event of an open-phase fault α-β and x-y planes happen to be coupled. The different harmonics are mapped into different subspaces: harmonics of the order $12n \pm 1$ (n = 1,2,3…) are mapped into the α-β plane (this include the fundamental component) whereas harmonics of the order $6n \pm 1$ (n = 1,3,5,…) are mapped into the x-y plane.

Assuming distributed windings and negligible spatial harmonics, the electrical equations of the machine can be expressed in stationary reference frame using the vector space decomposition (VSD) [1]:

$$\begin{aligned}
v_{\alpha s} &= \left(R_s + L_s\frac{d}{dt}\right) i_{\alpha s} + M\,\frac{di_{\alpha r}}{dt} \\
v_{\beta s} &= \left(R_s + L_s\frac{d}{dt}\right) i_{\beta s} + M\,\frac{di_{\beta r}}{dt} \\
v_{xs} &= \left(R_s + L_s\frac{d}{dt}\right) i_{xs} \\
v_{ys} &= \left(R_s + L_s\frac{d}{dt}\right) i_{ys} \\
v_{0+s} &= \left(R_s + L_s\frac{d}{dt}\right) i_{0+s} \\
v_{0-s} &= \left(R_s + L_s\frac{d}{dt}\right) i_{0-s} \\
0 &= \left(R_r + L_r\frac{d}{dt}\right) i_{\alpha r} + M\,\frac{di_{\alpha s}}{dt} + \omega_r L_r i_{\beta r} + \omega_r M i_{\beta s} \\
0 &= \left(R_r + L_r\frac{d}{dt}\right) i_{\beta r} + M\,\frac{di_{\beta s}}{dt} - \omega_r L_r i_{\alpha r} - \omega_r \cdot M i_{\alpha s}
\end{aligned} \tag{2}$$

where $L_s = L_{ls} + 3L_m$, $L_r = L_{lr} + 3L_m$, $M = 3L_m$ and ω_r is the rotor electrical speed ($\omega_r = p{\cdot}\omega_m$). Subscripts s and r denote stator and rotor variables, respectively.

Since the neutrals of the three-phase windings 1 and 2 are isolated, zero-sequence currents i_{0+} and i_{0-} cannot flow and are omitted from the analysis in what follows. On the other hand the x-y currents do not link the rotor side, resulting in circulating currents that only generate stator copper losses. Consequently, the torque production is purely related to the α-β subspace as in the three-phase case:

$$T_e = p \cdot M \cdot (i_{\beta r} \cdot i_{\alpha s} - i_{\alpha r} \cdot i_{\beta s}) \tag{3}$$

The machine is then driven in normal/healthy operation with null x-y currents and standard field-oriented control (FOC) for the regulation of the α-β (or d-q in rotating reference frame) currents. Apart from the need to include controllers to regulate the x-y currents, both the equations of the α-β plane and the control scheme remain the same as in three-phase machines.

B. Post-fault modes of operation

In the event of an open-circuit fault (OCF) it is necessary to detect and localize the fault before the control strategy is reconfigured [10]. After the fault detection delay, the aim of the fault-tolerant control is to preserve the pre-fault torque given in (3). As long as the α-β currents are kept unchanged it is possible to maintain a rotating circle-shaped magneto-motive force (MMF) and obtain a smooth post-fault operation [5]. However, the x-y currents can no longer be regulated to zero because the loss of one degree of freedom caused by the OCF couples the α-β and x-y current components. Assuming without lack of generality that a_1 is the open-circuited phase, it can be deduced from (1) that the x-current is now inversely proportional to the α-current:

$$i_{xs} = -i_{\alpha s} \tag{4}$$

One degree of freedom still remains and consequently a certain criterion must be chosen for the y-current reference. In principle the most intuitive choice is to maintain a null value:

$$i_{ys}^{*} = 0 \tag{5}$$

as in pre-fault condition, this resulting in a minimum loss (ML) mode of operation because the remaining VSD components are fixed (α-β currents to provide the necessary flux and torque and x-current due to the fault restriction). However, using the inverse Clarke transformation of (1), this selection results in heterogeneous phase currents with unequal amplitudes for the phase currents (Fig. 2a). If the current limit is set to the rated value I_n for all phases:

$$\mathrm{I_k} \leq \mathrm{I_n}\ \forall \mathrm{k}\ \in \{\text{Healthy phases}\} \tag{6}$$

then the phase with the higher current amplitude (black trace in Fig. 2a) sets the limit. However, the current amplitude in other healthy phases (red and green traces in Fig. 2a) is still well below the rated value and it results in a lower achievable torque production.

The other well-known strategy is to set the y-current reference so that phase currents have equal amplitudes, thus obtaining a maximum torque (MT) mode of operation where

all phase currents reach their rated values at the same time (Fig. 2b). Imposing the condition of equal peak values in the case under study, considering a circular shape for the α-β currents and including the restriction (4) into the Clarke transformation of (1), the resulting condition for the y-current injection becomes [10]:

$$i_{ys}^{*} = -i_{\beta s} \tag{7}$$

Even though the *y*-current injection of (7) slightly increases the machine and inverter losses, it is a mandatory procedure to maximize the post-fault achievable torque, and this lower derating is a main concern after the fault occurrence.

Either ML or MT criteria have been used in previous works independently, but not in conjunction. Since the maximum achievable torque is dependent on the mode of operation, the derating of the system is different for ML and MT criteria. The derating factor can be defined as the per unit value of the post-fault α-β current phasor modulus [8]:

$$a = \frac{|I_{\alpha\beta}|_{Post-fault}}{|I_{\alpha\beta}|_{Rated}} \tag{8}$$

The derating factor is shown in Fig. 3 for ML and MT modes of operation, resulting in a post-fault α-β current production of 55.5% (point B) and 57.7% (point A) for the asymmetrical six-phase motor ($\gamma = 30°$). The achievable torque in derated operation depends on how i_α and i_β are scaled down, but in the simple case where both components are equally decreased the torque limit is proportional to the square of the derating factor, obtaining two limits for ML and MT modes of operation:

$$T_{ML}^{max} = a_{ML}^2 T_n \tag{9}$$

$$T_{MT}^{max} = a_{MT}^2 T_n \tag{10}$$

If these torque limits are surpassed the drive enter an over-rated region with currents above I_n (Fig. 2c).

III. Braking Strategy in Post-Fault Situation

The ML and MT modes of operation defined by (5) and (7) fulfill the two main goals in normal motoring operation: maximize the achievable torque and minimize losses. The electrical torque from (3) is positive in these circumstances

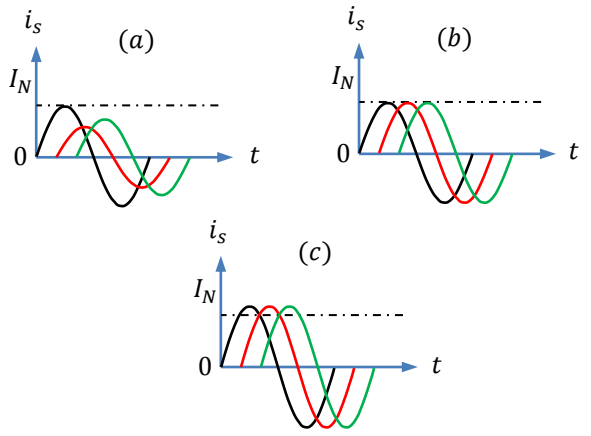

Fig. 2. Scheme of the post-fault phase currents waveforms in one set of three-phase windings: a) ML, b) MT (derated) and c) MT (over-rated).

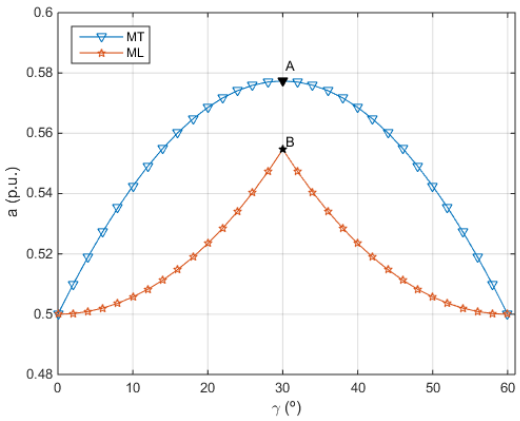

Fig. 3: Derating factor *a* versus spatial shifting angle γ for 1 OCF in two neutrals (2N) configuration.

and the shaft power is positive. In steady-state (i.e. $d\omega_r/dt$=0) the shaft torque equals the load torque and the friction, according to the mechanical equation of the motor:

$$T_{shaft} - T_{load} - B\omega_r = d\omega_r/dt \tag{11}$$

Nevertheless, when the motor needs to be braked and the load torque and friction are low enough, the deceleration can only be properly performed reversing the shaft power $T_{shaft} < 0$, as shown in Fig. 1a. When the motor and converter losses are not sufficiently high, this power eventually reaches the dc-link. If the topology does not allow a bidirectional power flow, as it is the case in many industrial drives equipped with diode front-end rectifiers, the active power is fully delivered to the dc-link capacitor and its voltage is dramatically increased [20-22].

In this scenario the only manner to speed up the deceleration and perform a quick braking transient is to increase the drive losses so that the reversed shaft power does not reach the dc-link (i.e. $P_{loss} > P_{shaft}$). In three-phase drives this can be achieved if the *d*-current is deliberately increased to elevate the motor losses and thus performed what is typically termed as *flux braking* [20].

However, the manipulation of the *d*-current influences to some extent the drive dynamics and issues related to saturation and over-magnetizing may take place [22]. Multiphase drives offer an additional possibility to independently manipulate the stator copper losses by proper regulation of the *x*-*y* components. This procedure has been implemented in [11] in healthy condition, confirming the capability of these secondary currents to enhance the braking transient without disturbing the flux/torque production. Although the stator and rotor resistances may vary due to the thermal effect, they are assumed to be constant for the calculation of the copper losses.

In the event of an OCF the motor loses one degree of freedom and the *x*-current is no longer controllable due to the restriction (4). It is however possible to manipulate stator copper losses through the regulation of the *y*-current:

$$i_{ys}^{*} = -\xi \cdot i_{\beta s} \tag{12}$$

Since (3) holds true after the fault occurrence, the torque is still independent of the *y*-current and it is possible to

implement a loss manipulation (LM) post-fault mode of operation without disturbing the flux/torque production.

The *y*-current injection can be regulated setting the value of $\xi > 0$. For $\xi = 0$ and $\xi = 1$ the motor is operated in ML and MT modes, respectively, but the LM mode can set $\xi > 1$ if required. Nonetheless a certain upper limit must be established for ξ in order to safely drive the motor without violating the thermal limits. In pre-fault condition the rated copper losses are equal to $6I_n^2$ so considering the copper losses in VSD variables [11] the current limit can be set by the condition:

$$i_{xs}^2 + i_{ys}^2 + i_{\alpha s}^2 + i_{\beta s}^2 = 6I_n^2 \tag{13}$$

Considering (4) and (12) one can set an upper limit for the *y*-current injection to guarantee that pre-fault copper losses are not surpassed:

$$\xi \le \xi_{max} = \sqrt{(6I_{max}^2 - 2i_{\alpha s}^2)/i_{\beta s}^2 - 1} \tag{14}$$

where the drive is operated with rated pre-fault copper losses if $I_{max} = I_n$, but the value of I_{max} can be further increased transiently according to the motor and converter overload capabilities [22].

IV. Variable Current Injection in Post-Fault Situation

A. Principle of operation.

Although the post-fault operation has been performed so far using a single criterion to set the *x*-*y* references [9-10], it follows from the description of the previous sections that the requirements of the drive are not the same in the whole range of operation. When the torque is positive and close to the post-fault operable limit of (10), the drive should be operated under MT mode with $\xi = 1$. If the torque falls below the limit set in (9), then it is no longer necessary to inject *y*-current and the drive should be operated under ML mode with $\xi = 0$ to promote efficiency. Finally, during braking transients the aim is to manipulate losses to achieve a positive dc-link power ($P_{DC} \ge 0$) and avoid capacitor overvoltage. Since the detection of the moment when the dc-link power is being reversed would require additional measurements, one can activate the LM mode when torque becomes negative and this keeps the procedure on the safe side (Fig. 4). While the torque is negative the LM mode injects *y*-current up to the limit ξ^{max} set in (14).

Fig. 5 shows an example of the different post-fault requirements of the drive according to the operation point. For $t < t_0$ the motor is driven at a speed n_1 with a load torque $T_1 \ge T_{ML}^{max}$, so the drive is operated under MT criterion. At time t_1 the load torque is reduced to a certain value T_2 where the y-current injection is no longer necessary ($0 \le T_2 \le T_{ML}^{max}$) and the drive is thus operated under ML criterion to maximize efficiency. After time t_1 the speed reference is decreased and the motor needs to be braked suddenly. If the ML mode is maintained, the dc-link power would become negative and in this moment the drive is switched to operate in LM mode, injecting a variable *y*-current for $t_1 \le t \le t_2$. The LM mode generates a variable *x*-*y* current dissipation that allows the motor to properly decelerate without putting the dc-link capacitor at risk. After the braking transient ($t \ge t_2$) it is no longer necessary to deliberately induce copper losses and the drives comes back to the ML mode. The suggested strategy combines MT, ML and LM modes aiming to fulfill all requirements in post-fault operation: maximizing the torque production, minimizing copper losses and keeping the dc-link voltage under control.

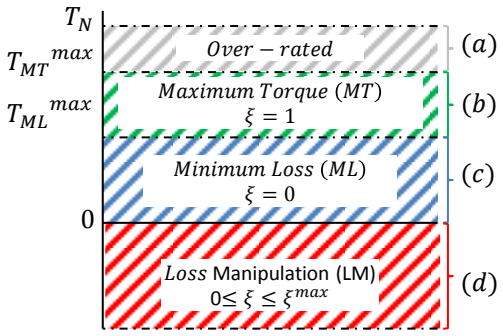

Fig. 4. Scheme of the different zones and modes of operation after the fault occurrence: a) Non-operable zone, b) MT zone ($\xi = 1$), c) ML zone $\xi = 0$) and d) LM zone ($0 \le \xi \le \xi^{max}$).

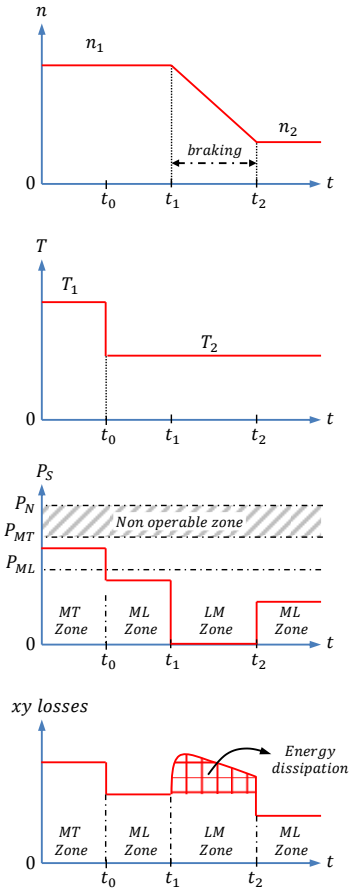

Fig. 5. Scheme of the post-fault operation in different zones: a) MT for $t < t_0$, b) ML for $t_0 < t < t_1$, a) LM for $t_1 < t < t_2$ and a) ML for $t > 2$.

The implementation of the conceptual idea of Fig. 4 into a high performance control scheme is described next.

B. Post-fault control with variable x-y current injection

The general scheme of the post-fault control is shown in Fig. 6a and it follows a standard FOC strategy with an outer speed loop and inner current loops. The *d*-current reference is set to a constant value $i_{ds}^{*} = i_{dsn}$ in order to operate at rated steady-state flux in the base-speed region and the *q*-current reference is obtained from the speed loop and is responsible for the torque production. Since the *d-q* current control is performed in a synchronous reference where the references are constant values in steady-state, it is sufficient to use single PI controllers to obtain the *d-q* voltage references. On the other hand, the post-fault *x-y* reference currents from (4) and (12) are non-constant values and there is no rotating frame where they become constant. Consequently, it is necessary to use resonant (double PI) controllers in order to properly track the non-constant *x-y* references that are set after the fault occurrence [8, 11]. This controller is implemented through double PI controllers in synchronous (using Park transformation $[D]$) and anti-synchronous directions (using the inverse Park transformation $[D]^{-1}$) and its output provide the *x-y* voltage references in stationary reference frame. The α-β and *x-y* voltage reference are transformed back to phase voltages (using the inverse Clarke's transformation $[T]^{-1}$) that are used as input for the carrier-based PWM stage.

The clue in the implementation of the global post-fault strategy is the determination of the *x-y* references, and specifically the determination of the variable injection factor ξ that defines the *y*-current injection according to (14). The zones defined in Fig. 4 are implemented following the flowchart of Fig. 6b, where the different values of ξ are obtained as a function of the electrical torque. Above the maximum post-fault achievable torque the motor operates in expense of a poorer dynamic performance. Below this limit over-rated condition and it is necessary to saturate the *q*-reference current to keep the motor within rated value at the the motor transits to the MT, ML and LM zones according to Fig. 4, allowing the motor to maximize the torque production, improve efficiency and keep the unidirectional power flow. The latter is achieved using the loss controller depicted in Fig. 6c. The aim of the controller is to maintain the stator power positive (or above a certain threshold) to avoid the power reversal and the eventual breakdown of the dc-link capacitor. It is implemented using a low-pass filter (with a cut-off frequency of 250 Hz), an anti-windup PI controller and the saturated value of ξ in (14).

V. Experimental Results

A. Test Bench

The different elements of the test rig that has been used for the experimental testing is shown in Fig. 7. The six-phase drive consists of an asymmetrical six-phase induction machine driven by conventional two-level three-phase VSCs from Semikron (SKS22F modules). Ac-time domain and stand-still with inverter supply tests [23-24] have been used to determine the parameters of the custom-built multiphase machine. The obtained parameters together with the rated values of the six-phase motor are included in table I, whereas the gains of the PI controllers shown in Fig. 6 are listed in table II.

The VSCs are connected to a single dc power supply and the control actions are performed by a digital signal processor (TMS320F28335 from Texas Instruments, TI). The control unit is programmed using a JTAG and the TI proprietary software called Code Composer Studio. Four hall-effect sensors (LEM LAH 25-NP) and a digital encoder (GHM510296R/2500) have been used to obtain the current and speed measurements, respectively. A dc machine is coupled to the shaft of the six-phase induction motor in order to perform load tests. The armature of the dc machine is connected to a variable passive *R* load that dissipates the power and the load torque is consequently speed-dependent.

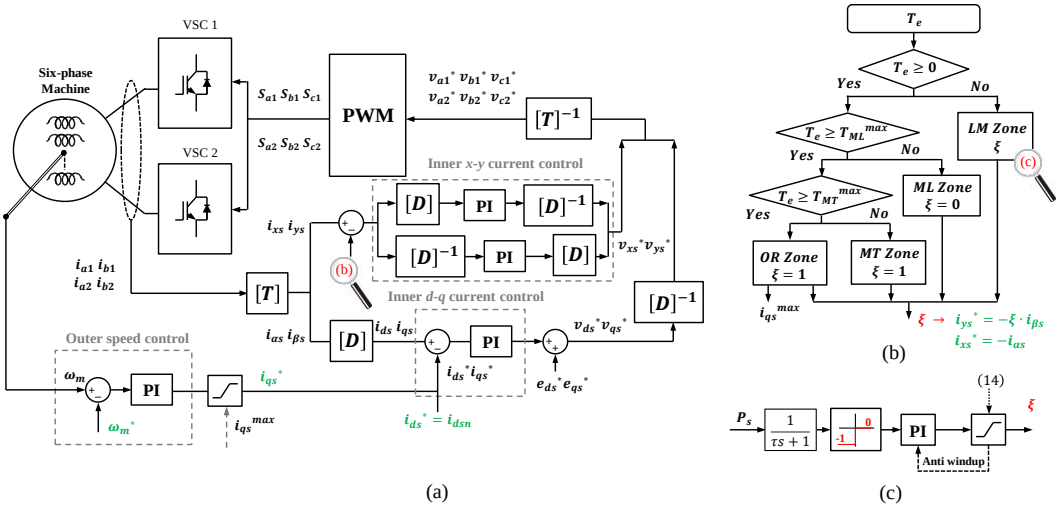

Fig. 6. Control scheme of the global post-fault strategy: a) FOC using resonant controllers for the *x-y* currents, b) Flowchart indicating the conditions to enter ML, MT and LM zones and c) LM controller.

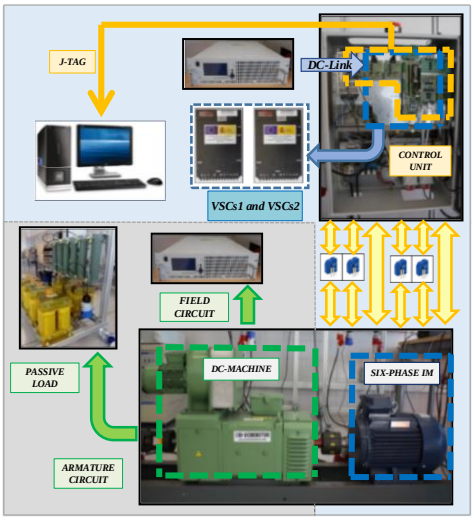

Fig. 7: Scheme of the test bench used for the experimental results.

TABLE I
INDUCTION MOTOR PARAMETERS AND RATED VALUES

$Power\ (kW)$	0.4
$I_{peak}(A)$	2.6
$i_d(A)$	1.1
$i_q(A)$	3
$\omega_m(rpm)$	1000
$R_s(\Omega)$	4.2
$R_r(\Omega)$	2
$L_m\ (mH)$	420
$L_{ls}\ (mH)$	4.2
$L_{lr}\ (mH)$	55

TABLE II
GAINS OF THE PI CONTROLLERS

Controller	K_p	K_i
PI ω	0.85	0.5
PI d current	100	215
PI q current	35.5	235
PI x current	20	70
PI y current	20	70
PI ξ	0.1	3

B. Experimental Results

This section experimentally verifies the performance of the global post-fault strategy and the transition from MT, ML and LM zones (Fig. 6b) when phase a_1 is open-circuited. The results are split into four tests: test 1 verifies the transition from MT to ML mode, test 2 shows the transition from ML to LM mode and vice versa, test 3 compares the stator copper losses in MT and ML modes and test 4 compares the braking transients with and without activating the LM mode.

In test 1 (Fig. 8) the machine is initially in steady-state providing an electrical torque above the threshold T_{ML}^{max} of (9) and it is thus operated in MT mode. The motor speed and d-q currents are constant (Fig. 8a and 8b, respectively), and the currents correspond to the MT criterion at $t = 4s$ (zoom-in plot in Fig. 8c) with the injection of y-current defined in (7) that corresponds with $\xi = 1$ (Fig. 8d). At time $t = 5s$ the motor is decelerated but the electrical torque always remain positive, thus indicating that the stator power is not reversed and it is not necessary to manipulate the losses during this transient (LM mode is not activated). However, since the load of the motor is dependent on the speed because it is coupled to a dc-generator, during the braking the electrical torque falls below the threshold T_{ML}^{max} and the transition to ML occurs. The transition is almost instantaneous and the value of ξ drops to zero (Fig. 8d) causing the phase current to be unbalanced (zoom-in plot in Fig. 8c) as it is characteristic in the ML mode of operation. Efficiency is favored with this transition since the null injection of y-current decreases the copper losses. It can be observed in test 1 that the injection of y-current is only activated when necessary and in this manner it is possible to fully exploit the post-fault torque capability (operating up to the T_{MT}^{max} limit) and promote efficiency. Since the y-current is not involved in the energy conversion process the transition can be done quickly and with no effect on the drive dynamics.

Test 2 (Fig. 9) explores the excursion from ML to LM mode during braking transients. The machine is initially operated in ML mode with $\xi = 0$ because the torque is below the threshold T_{ML}^{max}. The machine is drive in steady-state with constant speed, d-q currents and torque/power when it is commended to decelerate in a ramp-wise manner at $t = 5s$. Since the machine is lightly loaded and the slope of the ramp sufficiently steep, the torque falls before the threshold and the LM mode is activated. For security reasons the threshold for the activation of the LM mode, which is zero in Fig. 6b, is set to a low but positive value in the experiments. From $t = 5$ to $7\ s$, approximately, the LM y-current injection is regulated by the controller of Fig. 6b, thus resulting in variable values of the current injection factor (zoom-in plot in Fig. 9d). The value of ξ is increased during the braking transient to keep the stator power above the threshold (shown in Fig. 9d with a blue discontinuous trace), but the upper limit for the y-current injection set in (14) is never reached. The motor dynamics is not affected (see speed and d-q currents in Fig. 9a and 9b, respectively) but the variable y-current injection provided by the LM mode maintains the stator power under control and avoids the reversal of the power that might eventually cause over-voltages in the dc-link capacitor. The y-current injection of course spoils efficiency but these extra copper losses are only transiently induced and as soon as the braking process is ended the drive returns to the ML mode with $\xi = 0$ (zoom-in plot in Fig.9d) and unbalanced phase currents (zoom-in plot in Fig.9c). Test 2 shows that it is possible to promote efficiency in steady-state using the ML mode but to avoid power reversal during braking transients following a post-fault LM strategy.

Tests 3 firstly drives the machine from 250 to 150 rpm with MT (red trace in Fig. 10) and then the same test is repeated with ML (blue trace in Fig. 10), showing that the stator copper losses can be effectively reduced by activating the ML criterion when the torque is below the limit set in (9) following the procedure shown in Fig. 6b.

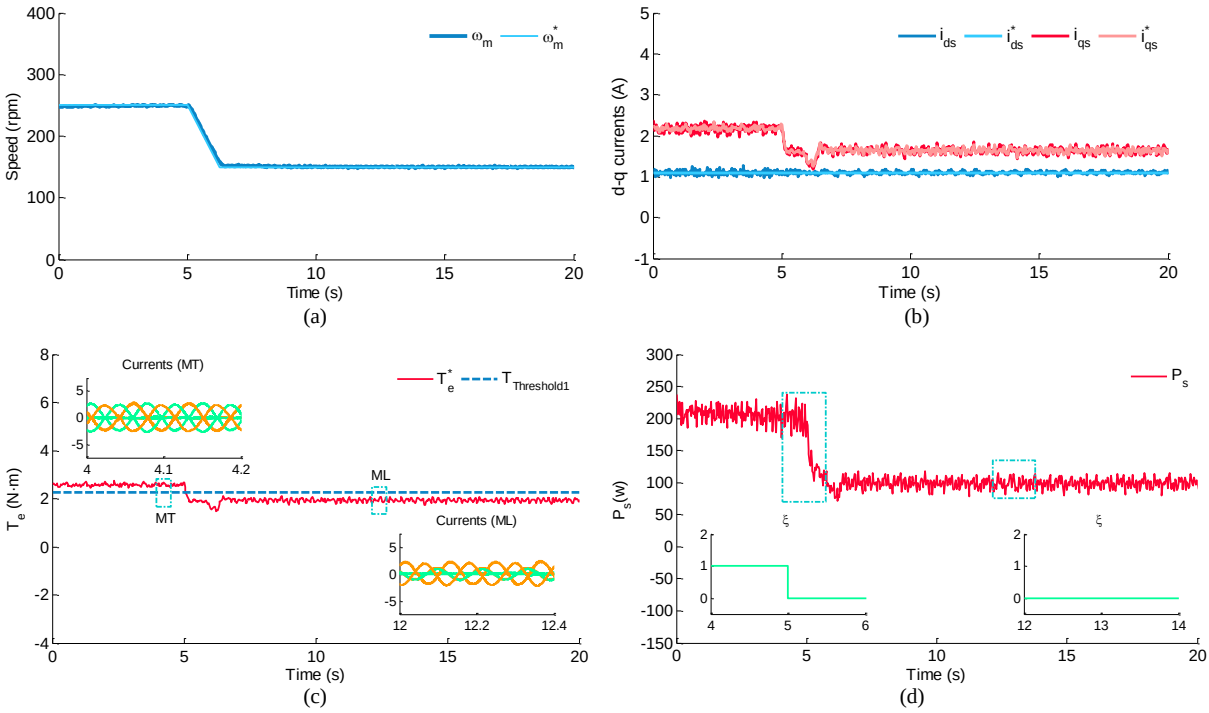

Fig. 8. Tests 1, transition from MT to ML: (a) motor speed, (b) *d-q* currents, (c) torque and zoom-in currents, (d) current injection factor ξ.

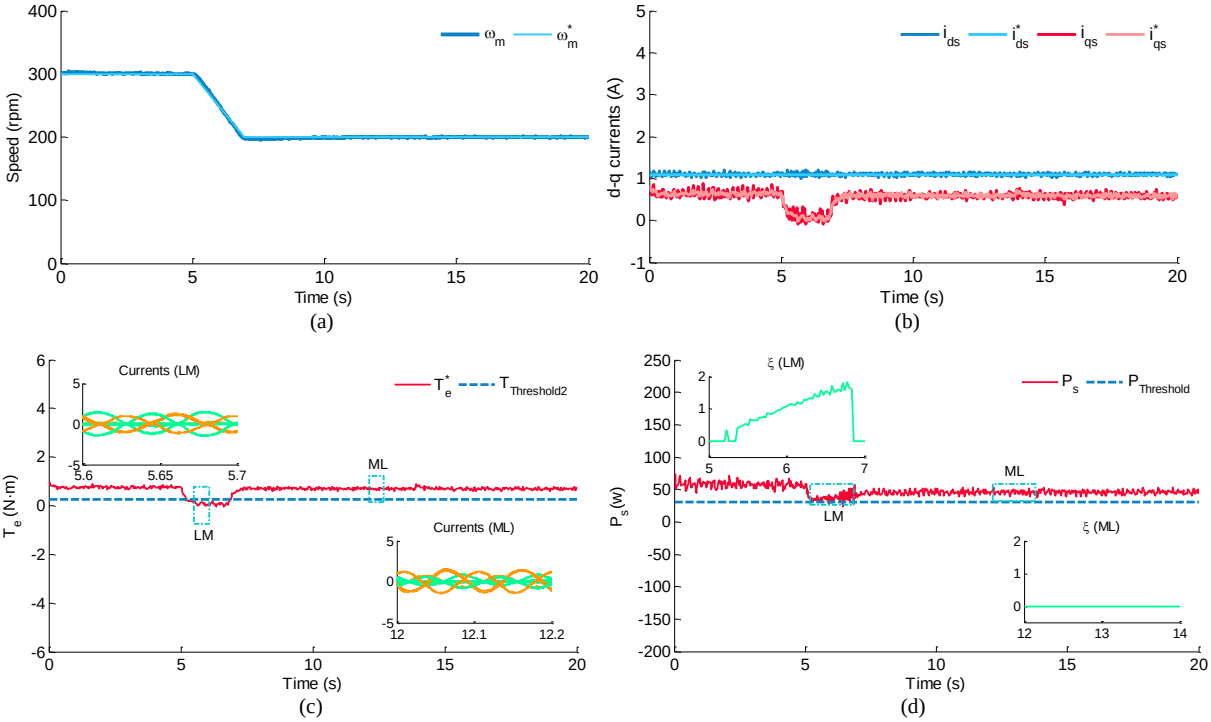

Fig. 9: Test 2 - Transition from LM to ML: (a) motor speed, (b) *d-q* currents, (c) torque and zoom-in currents, (d) stator power and zoom-in ξ.

Test 4 finally compares the braking transient (decelerating from 300 to 200 rpm) with and without activating the LM mode (Fig. 11). In Fig. 11a it can be observed that the activation of the LM mode maintains the stator power above the threshold (depicted as a horizontal blue line). On the other hand, if the LM mode is not activates the stator power repetitively falls below the threshold, eventually allowing the active power to reach the dc-link and cause an overvoltage in the capacitor. The comparison shown in Fig. 11 confirms the capability of the LM mode to keep the stator power within safe limits during sharp braking transients.

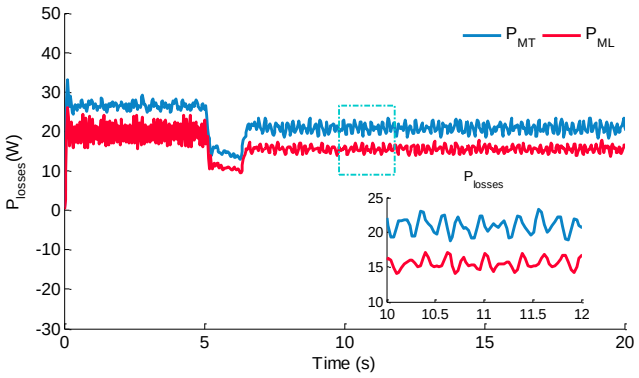

Fig. 10. Tests 3, comparison of the losses with MT (blue trace) and ML (red trace) criteria

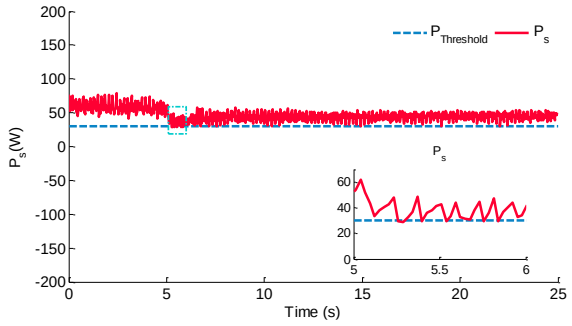

(a)

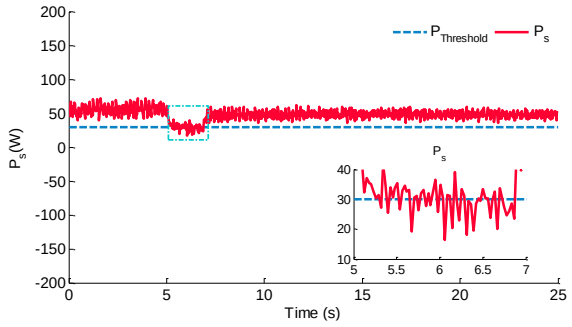

(b)

Fig. 11. Tests 4, comparison of the performance with and without activating the LM strategy: (a) Stator power with LM, (b) Stator power without LM. Stator power threshold is shown in blue trace.

It must be highlighted that the inverter losses are not considered in the control scheme of Fig. 6. Nevertheless, the inverter losses would help to avoid the flow of the active power to the dc-link. In other words, if the stator power is slightly negative but lower than the inverter losses, the power would not reach the dc-link since the converter is also helping to dissipate some active power. In any case setting the stator power threshold at zero (as shown in Fig. 6) happens to be on the safe side and provides a simple manner to avoid the capacitor overvoltage. Taking into account that the LM mode is only briefly activated during sharp decelerations, the intentionally induced inefficiency in the machine/inverter has a limited impact on the overall losses but enhances the braking capability of the drive.

To sum up, tests 1 to 4 show that it is possible to use a global post-fault strategy that:

i) Fully exploits the torque capability (MT) when the limit in (9) is surpassed and the *y*-current is set as in (7).

ii) Reduces the copper losses (ML) when the drive is operated below the limit in (9) and the stator power is above the threshold of the LM technique.

iii) Enhances braking transients (LM) because the induced losses in the LM strategy allows to further decelerate the machine without exceeding the power limit and putting the dc-link capacitor at risk.

The transition between the different states (zones (b), (c) and (d) in Fig. 4) of the global strategy defined in Fig. 6b is performed almost instantaneously and with no adverse effects on the drive dynamics.

VI. Conclusions

Electrical drives equipped with diode front-end converters cannot perform regenerative braking and the only manner to speed up the deceleration process is to increase the system losses. After a single open-phase fault, six-phase drives still have one remaining degree of freedom (*y*-current in the case of phase a_1) and it can be used to increase the stator copper losses and thus enhance the braking capability of the drive with no adverse effects on the dc-link capacitor. The transient injection of the *y*-current allows a loss manipulation mode of operation with no disturbance of the drive dynamics, maintaining the unidirectional power flow with the addition of a single controller.

Since the injection of the *y*-current also has an impact on the efficiency and maximum post-fault achievable torque, it is possible to obtain an optimal performance by combining the transient loss manipulation mode with another two steady-state modes that minimize the copper losses and maximize the torque production. The global strategy does not add much complexity to the fault-tolerant control scheme but provides a good performance in the whole range of operation.

References

[1] E. Levi, R. Bojoi, F. Profumo, H.A. Toliyat and S. Williamson, "Multiphase induction motor drives - A technology status review," *IET Electric Power Applications*, vol. 1, no. 4, pp. 489-516, 2007.

[2] E. Levi, F. Barrero and M.J. Duran, "Multiphase machines and drives – Revisited," *IEEE Trans. Ind. Electron.*, vol 63, no. 1, pp. 429-432, 2016.

[3] E. Levi, "Advances in converter control and innovative exploitation of additional degrees of freedom for multiphase machines," *IEEE Trans. Ind. Electron.*, vol 63, no. 1, pp. 433-448, 2016.

[4] F. Barrero and M.J. Duran, "Recent advances in the design, modeling and control of multiphase machines – Part 1," *IEEE Trans. Ind. Electron.*, vol 63, no. 1, pp. 449-458, 2016.

[5] M.J. Duran and F. Barrero, "Recent advances in the design, modeling and control of multiphase machines – Part 2," *IEEE Trans. Ind. Electron.*, vol 63, no. 1, pp. 459-468, 2016.

[6] H.S. Che, E. Levi, M. Jones, M.J. Duran, W.P. Hew, and N.A. Rahim, "Operation of a six-phase induction machine using series-connected machine-side converters," *IEEE Trans. Ind. Electron.*, vol. 61, no. 1, pp. 164-176, 2014.

[7] I. Subotic, N. Bodo, E. Levi and M. Jones, "Onboard integrated battery charger for EVs using an asymmetrical nine-Phase Machine," *IEEE Trans. Ind. Electron.*, vol 62, no. 5, pp. 3285-3295, 2015.

[8] H.S. Che, M.J. Duran, E. Levi, M. Jones, W.P. Hew and N.A. Rahim, "Post-fault operation of an asymmetrical six-phase induction machine with single and two isolated neutral points," *IEEE Trans. on Power Electronics*, vol. 29, no. 10, pp. 5406-5416, 2014.

[9] I. Gonzalez-Prieto, M.J. Duran, F. Barrero, M. Bermudez and H. Guzman, "Impact of post-fault flux adaptation on six-phase induction motor drives with parallel converters," *IEEE Trans. on Power Electronics, early access*, DOI: 10.1109/TPEL.2016.2533719, 2016.

[10] H. Guzman, M.J. Duran, F. Barrero, B. Bogado, I. Gonzalez-Prieto and M.R. Arahal, "Comparative study of predictive and resonant controllers in fault-tolerant five-phase induction motor drives," *IEEE Trans. Ind. Electron.*, vol. 63, no. 1, pp. 606-617, 2016.

[11] M.J. Duran, I. Gonzalez-Prieto, F. Barrero, M. Mengoni, L. Zarri and E. Levi, "A simple braking method for six-phase induction motor drives with diode front-end rectifier," *Industrial Electronics Society, IECON 2015 – 41st Annual Conference of the IEEE*, 9-12 Nov. 2015.

[12] "Gamesa 5.0 MW" Gamesa Technological Corporation S.A., 2016. Online available: http://www.gamesacorp.com/recursos/doc/productos-servicios/aerogeneradores/catalogo-g10x-45mw.pdf

[13] C. Ditmanson, P. Hein, S. Kolb, J. Mölck and S. Bernet, "A new nodular flux-switching permanent-magnet drive for large wind turbines," *IEEE Ind. Appl. Mag.*, vol. 50, no. 6, pp. 3787-3794, 2014.

[14] E. Jung, H. Yoo, S. Sul, H. Choi and Y. Choi, "A nine-phase permanent-magnet motor drive system for an ultrahigh-speed elevator," *IEEE Trans. Ind. Appl.*, vol. 48, no. 3, pp. 987-995, 2012.

[15] W. Cao, B.C. Mecrow, G.J. Atkinson, J.W. Bennett and D.J. Atkinson, "Overview of electric motor technologies used for more electric aircraft (MEA)" *IEEE Trans. on Ind. Electron.*, vol. 59, no. 9, pp. 3523-3531, 2012.

[16] L. Zarri, M. Mengoni, Y. Gritli, A. Tani, F. Filippetti, G. Serra and D. Casadei, "Detection and localization of stator resistance dissymmetry based on multiple reference frame controllers in multiphase induction motor drives," IEEE Trans. Ind. Electron., vol. 60, no. 8, pp. 3506-3518, 2013.

[17] A.S. Abdel-Khalik, M.I. Masoud, S. Ahmed and A. Massoud, "Calculation of derating factors based on steady-state unbalanced multiphase induction machine model under open phase(s) and optimal winding currents," *Electric Power System Research*, vol. 106, pp. 214-225, 2014.

[18] S. Dwari and L. Parsa, "An optimal control technique for multiphase PM machines under open-circuit faults," *IEEE Trans. Ind. Electron.*, vol. 55, no. 5, 2008.

[19] Kestelyn and E. Semail, "A vectorial approach for generation of optimal current references for multiphase permanent-magnet synchronous machines in real time," *IEEE Trans. Ind. Electron.*, vol. 58, no. 11, pp. 5057-5065, 2011.

[20] ABB Drives Group. *Technical guide No. 8. Electrical braking.* Chapter 1, pp. 7-9, 2011.

[21] M. Hinkkanen and J. Luomi, "Braking scheme for vector controlled induction motor drives equipped with diode rectifier without braking resistor," *IEEE Trans. on Ind. Appl.*, vol. 42, no. 5, pp. 1257-1263, 2006.

[22] J. Jiang and J. Holtz, " An efficient braking method for vector controlled AC drives with a diode rectifier front end", *IEEE Trans. on Industry Appl*ications vol. 37, no. 5, pp. 1299-1307, 2001.

[23] A.G. Yepes, J.A. Riveros, J. Doval-Gandoy, F. Barrero, O. Lopez, B. Bogado, M. Jones and E. Levi, "Parameter Identification of Multiphase Induction Machines With Distributed Windings—Part 1: Sinusoidal Excitation Methods," *IEEE Trans. Energy Convers.*, vol. 27, no. 4, pp. 1056-1066, 2012.

[24] J.A. Riveros, A.G. Yepes, F. Barrero, J. Doval-Gandoy, B. Bogado, O. Lopez, M. Jones and E. Levi, "Parameter Identification of Multiphase Induction Machines With Distributed Windings—Part 2: Time-Domain Techniques," *IEEE Trans. Energy Convers.*, vol. 27, no. 4, pp. 1067-1077, 2012.

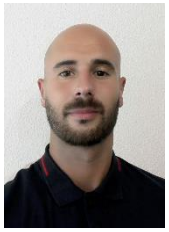

Ignacio Gonzalez Prieto was born in Malaga, Spain, in 1987. He received the Industrial Engineer and M. Sc. degrees from the University of Malaga, Spain, in 2012 and 2013, respectively. He obtained the PhD degree in Electronic Engineering from the University of Seville, Spain, in 2016. His research interests include multiphase machines, wind energy systems and electrical vehicles.

Mario J. Duran was born in Málaga, Spain, in 1975. He received the M.Sc. and Ph.D. degrees in Electrical Engineering from the University of Málaga Spain, in 1999 and 2003, respectively. He is currently an Associate Professor with the Department of Electrical Engineering at the University of Málaga. His research interests include modeling and control of multiphase drives and renewable energies conversion systems.

Federico Barrero (M'04–SM'05) received the M.Sc. and Ph.D. degrees in electrical and electronic engineering from the University of Seville, Seville, Spain, in 1992 and 1998, respectively. In 1992, he joined the Department of Electronic Engineering, University of Seville, where he is currently an Associate Professor. Dr. Barrero received the Best Paper Awards from the IEEE Transactions on Industrial Electronics for 2009 and from the IET Electric Power Applications for 2010-2011.